Quantum phase transition and quench dynamics in the two-mode Rabi model

Li-Tuo Shen, Jing-Wen Yang, Zhi-Rong Zhong,* Zhen-Biao Yang,† and Shi-Biao Zheng
Fujian Key Laboratory of Quantum Information and Quantum Optics, College of Physics and Information Engineering, Fuzhou University, Fuzhou, Fujian 350116, China

(Received 22 July 2021; accepted 22 November 2021; published 8 December 2021)

The second-order quantum phase transition and quench dynamics in the two-mode Rabi model are investigated. We propose a diagonalization approach of jointly using a beam-splitter operator and a squeezed operator for each effective low-energy Hamiltonian when the ratio of the qubit transition frequency to the oscillator frequency approximates infinity. Eigenenergy and eigenstate of the normal and superradiant phases in the system are analytically derived, demonstrating the second-order quantum phase transition at a critical point. This critical point means that the requirement of coupling strength between the qubit and two oscillators is largely loosened by joint effect of two modes when compared with the standard Rabi model. The universal scaling between residual energy and quench time from $\tau^{-\frac{1}{3}}$ to τ^{-2} is confirmed.

DOI: 10.1103/PhysRevA.104.063703

I. INTRODUCTION

The quantum phase transition is an important issue in the area of quantum optics and condensed-matter physics [1–14]. Different from the classical phase transition, which usually appears at finite temperature, a quantum phase transition always appears at zero temperature. Traditional studies of the quantum phase transition [15–17] mainly focus on the thermodynamic limit, where the number of microparticle becomes infinity, for example, the Dicke model [18].

However, a recent theoretical study [19] shows that a second-order quantum phase transition can occur under a special frequency ratio even when the system only contains a qubit and an oscillator, i.e., the Rabi model [20]. Recently, a trapped-ion experiment [21] using a $^{171}Yb^{+}$ ion in a Paul trap observed this quantum phase transition, which opens up a new window for controllable study of the quantum phase transition without requiring the thermodynamic limit.

To reveal the crossover effect between classical and quantum worlds, the natural question of when the oscillator number increases for the Rabi model whether the second-order quantum phase transition still exists remains an open question. A recent study [22] investigated the dissipative phase transition based on the two-mode Rabi model by using the mean-field approximation. Although this study demonstrated that the PT symmetry breaking resulted in plentiful phase transitions and a phase diagram, they did not definitely analyze whether the second-order quantum phase transition existed. Other works [23,24] solved the analytical ground state of the two-mode Rabi model but only discussed the entanglement and nonclassical property.

When a slow quench approaches the critical point of quantum phase transition, for example, changing the qubit-oscillator coupling strength by slowly tuning the external magnetic field, the spectral gap is closing and the adiabaticity of dynamics breaks despite the quench rate [25–32]. The work of Ref. [19] has proved that the transition relation of universal scaling between residual energy and quench time in the standard Rabi model, but whether this transition relation of universal scaling keeps the same in the two-mode Rabi model is still unknown.

To investigate the second-order quantum phase transition and quench dynamics in the two-mode Rabi model, we here propose a diagonalization approach of jointly using a beam-splitter operator and a squeezed operator and find a special transformation operator mapping the original Hamiltonian into an effective two-mode Hamiltonian when the ratio of the qubit transition frequency to each oscillator frequency approximates infinity. The analytical eigenenergy and eigenstate of the normal phase and superradiant phase are derived, respectively. We demonstrate that the ground state undergoes a second-order quantum phase transition at a critical point, which is largely loosened by the joint effect of two modes other than the standard Rabi model. In the quench dynamics, we consider the main finite-frequency correction and analytically derive the universal scaling between residual energy and quench time. The two-mode Rabi model is interesting because it adds a deeper insight of understanding the quantum phase transition, explaining the role that the mode number plays on the quantum phase transition, revealing a new critical point of quantum phase transition.

II. QUANTUM PHASE TRANSITION

As shown in Fig. 1, the Hamiltonian of a two-mode Rabi model is ($\hbar = 1$) [22]

$$H = \omega_a a^\dagger a + \omega_b b^\dagger b + \frac{\Omega}{2}\sigma_z - \lambda_a(a^\dagger + a)\sigma_x - \lambda_b(b^\dagger + b)\sigma_x, \tag{1}$$

*zhirz@fzu.edu.cn
†zbyang@fzu.edu.cn

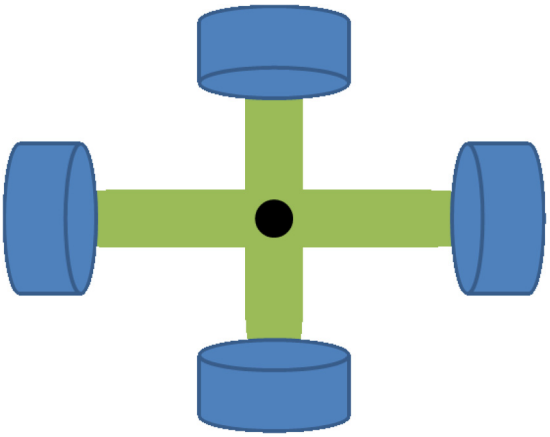

FIG. 1. Setup of a two-mode Rabi model. Two green-bold lines represent two modes a and b, respectively. Black-solid dot represents a qubit.

where σ_x and σ_z are Pauli matrices of a qubit. $a^\dagger(b^\dagger)$ and $a(b)$ are the creation and annihilation operators of the field mode $a(b)$, respectively. $\omega_a(\omega_b)$ is the $a(b)$ mode's frequency. Ω is the transition frequency of the qubit. $\lambda_a(\lambda_b)$ is the coupling strength between $a(b)$ mode and the qubit. For simplicity, $\omega_a = \omega_b = \omega_0$ and $\lambda_a = \lambda_b = \lambda$ are set. $|\downarrow\rangle$ and $|\uparrow\rangle$ are the high- and low-energy eigenstates of σ_z, respectively. $|m\rangle_{a(b)}$ ($m \in \mathbf{N}$) is the eigenstate of $a^\dagger a(b^\dagger b)$. The parity operator $\Pi = e^{i\pi[a^\dagger a + b^\dagger b + \frac{1}{2}(1+\sigma_z)]}$ measures an even-odd parity of total excitation number, which commutes with H. The approach of investigating phase transition in Ref. [22] is the mean-field approximation, which is applicable only when the whole system approaches the classical regime but fails when the system is completely quantum. To solve this problem, we propose a diagonalization method to investigate the quantum phase transition and find more interesting results.

In the limit $\frac{\Omega}{\omega_0} \to \infty$, we find a unitary transformation $U_T = e^{\frac{\lambda}{\Omega}(a^\dagger + a + b^\dagger + b)(\sigma_+ - \sigma_-)}$ to remove the coupling terms between the qubit's subspaces $\{|\downarrow\rangle\}$ and $\{|\uparrow\rangle\}$, i.e., $H_T = U_T^\dagger H U_T$, where $\sigma_+ = |\uparrow\rangle\langle\downarrow|$ and $\sigma_- = |\downarrow\rangle\langle\uparrow|$. When H_T is projected into $\{|\downarrow\rangle\}$, an effective two-mode Hamiltonian in normal phase is obtained:

$$H_{np} = \omega_0(a^\dagger a + b^\dagger b) - \frac{\lambda^2}{\Omega}(a^\dagger + a + b^\dagger + b)^2 - \frac{\Omega}{2}. \quad (2)$$

The main obstacle here is to diagonalize H_{np} in the two-mode subspace. It is obvious that H_{np} has a cross-interaction term between two modes, i.e., $(a^\dagger + a)(b^\dagger + b)$, and this similar structure of H_{np} has been used to calculate the quantum phase transition and chaos of the Dicke model in Ref. [18]. However, the Bogoliubov transformation method of Ref. [18] lacks a universal form of eigenstate in the original Hilbert space, which is hard to generalize to investigate the time-dependent dynamics here, for example, quench dynamics.

To settle this problem, we propose a diagonalization method for H_{np}. By jointly using a beam-splitter operator $U_\theta = e^{\theta(a^\dagger b - a b^\dagger)}$ and a squeezed operator $U_s = e^{\frac{s}{2}(a^{\dagger 2} - a^2)}$ (θ and s are two parameters determined in the Appendix), H_{np} is diagonalized as

$$H'_{np} = \omega_0\sqrt{1-2g^2}a^\dagger a + \omega_0 b^\dagger b + \frac{\omega_0}{2}\sqrt{1-2g^2} - \frac{\omega_0}{2} - \frac{\Omega}{2}, \quad (3)$$

with excitation energies $\epsilon_{np,a} = \omega_0\sqrt{1-2g^2}$ for the a oscillator and $\epsilon_{np,b} = \omega_0$ for the b oscillator, where $g = \frac{2\lambda}{\sqrt{\omega_0\Omega}}$. $\epsilon_{np,b}$ is a definitely real value for any non-negative g, but $\epsilon_{np,a}$ is real only for $0 \leqslant g \leqslant \frac{\sqrt{2}}{2}$ and imaginary only for $g > \frac{\sqrt{2}}{2}$, indicating that the quantum phase transition happens at a critical point $g_c = \frac{\sqrt{2}}{2}$. The universal form of low-energy eigenstates of H_{np} for $g \leqslant \frac{\sqrt{2}}{2}$ is $|\phi_{np}^{m,n}(g)\rangle = U_\theta^\dagger U_s^\dagger |m, n\rangle_{a,b}|\downarrow\rangle$, with $\theta = \frac{\pi}{4}$ and $s = \frac{1}{4}\ln(1-2g^2)$. Note that $|\phi_{G,np}\rangle = U_T^\dagger U_\theta^\dagger U_s^\dagger |0,0\rangle_{a,b}|\downarrow\rangle$ is the ground state in normal phase and the ground-state energy is $E_{0,np} = \frac{\omega_0}{2}\sqrt{1-2g^2} - \frac{\omega_0}{2} - \frac{\Omega}{2}$.

However, if another beam-splitter operator $U_{\theta'} = e^{\theta'(a^\dagger b - a b^\dagger)}$ and another squeezed operator $U'_s = e^{\frac{s}{2}(b^{\dagger 2} - b^2)}$ are jointly used, where $\theta' = -\frac{\pi}{4}$, H_{np} is diagonalized as $H''_{np} = \omega_0 a^\dagger a + \omega_0\sqrt{1-2g^2}b^\dagger b + \frac{\omega_0}{2}\sqrt{1-2g^2} - \frac{\omega_0}{2} - \frac{\Omega}{2}$, where excitation energies are $\epsilon'_{np,a} = \omega_0$ for the a oscillator and $\epsilon'_{np,b} = \omega_0\sqrt{1-2g^2}$ for the b oscillator. The ground state in normal phase becomes $|\phi'_{G,np}\rangle = U_T^\dagger U_{\theta'}^\dagger U_s'^\dagger |0,0\rangle_{a,b}|\downarrow\rangle$, but its ground-state energy is still $E_{0,np}$. The original Hamiltonian (1) is invariant under the interchange $a \leftrightarrow b$. This symmetry is broken when the squeezing operator is employed, giving rise to different excitation energies. But since two squeezed extents are the same, the ground-state energy is not influenced by the broken symmetry, which is demonstrated from Eq. (A1) to Eq. (A13) in the Appendix.

When $g > \frac{\sqrt{2}}{2}$, two oscillators are macroscopically occupied and the ground state comes into the superradiant phase. We transform the original Hamiltonian by displacing two field modes a and b with displacement operators $D_a(\alpha) = e^{\alpha(a^\dagger - a)}$ and $D_b(\beta) = e^{\beta(b^\dagger - b)}$, respectively. With the choice of displacement $\alpha = \beta = \sqrt{\frac{\Omega}{16\omega_0 g^2}(4g^4 - 1)}$, the displaced Hamiltonian can be written as the same formation of Eq. (1),

$$H_D = \omega_0(a^\dagger a + b^\dagger b) + \frac{\tilde{\Omega}}{2}\tilde{\sigma}_z - \tilde{\lambda}(a^\dagger + a + b^\dagger + b)\tilde{\sigma}_x + \frac{2\lambda^2}{\omega_0} - \frac{\omega_0\Omega^2}{32\lambda^2}, \quad (4)$$

where the revolved bases are $\tilde{\sigma}_z = \frac{1}{2g^2}(|\uparrow\rangle\langle\uparrow| - |\downarrow\rangle\langle\downarrow|) - \sqrt{1-\frac{1}{4g^4}}(|\uparrow\rangle\langle\downarrow| + |\downarrow\rangle\langle\uparrow|)$ and $\tilde{\sigma}_x = \sqrt{1-\frac{1}{4g^4}}(|\uparrow\rangle\langle\uparrow| - |\downarrow\rangle\langle\downarrow|) + \frac{1}{2g^2}(|\uparrow\rangle\langle\downarrow| + |\downarrow\rangle\langle\uparrow|)$, with the rescaled frequency $\tilde{\Omega} = \frac{8\lambda^2}{\omega_0}$ and the rescaled coupling strength $\tilde{\lambda} = \frac{\omega_0\Omega}{8\lambda}$. Based on the same procedure of deriving H_{np}, an effective two-mode Hamiltonian in superradiant phase is obtained,

$$H_{sp} = \omega_0(a^\dagger a + b^\dagger b) - \frac{\omega_0^3\Omega^2}{512\lambda^4}(a^\dagger + a + b^\dagger + b)^2 - \frac{2\lambda^2}{\omega_0} - \frac{\omega_0\Omega^2}{32\lambda^2}, \quad (5)$$

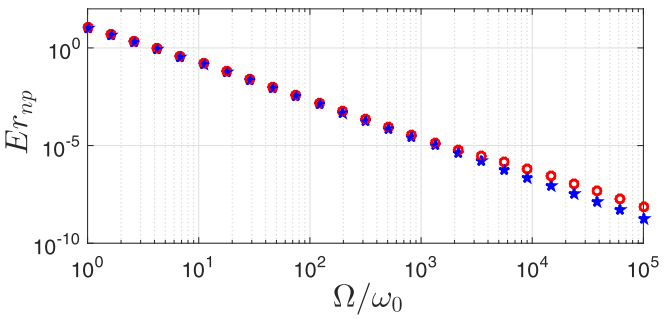

FIG. 2. Relative errors Er_{np} of ground-state energy between the numerical solution of H and analytical solution of $\tilde{H}_T$ at $g = \frac{\sqrt{2}}{4}$ (blue star) and $g = \frac{\sqrt{2}}{2}$ (red circle). The units of horizontal coordinate and vertical coordinate are dimensionless and ω_0, respectively.

which can be diagonalized by U_θ and $U_{\tilde{s}} = e^{\frac{\tilde{s}}{2}(a^{\dagger 2} - a^2)}$, where $\tilde{s} = \frac{1}{4}\ln[1-(4g^4)^{-1}]$ is the rescaled squeezed parameter. Excitation energies of H_{sp} for the a and b oscillator are $\epsilon_{sp,a} = \omega_0\sqrt{1-(4g^4)^{-1}}$ and $\epsilon_{sp,b} = \omega_0$, respectively, which are both real for $g > \frac{\sqrt{2}}{2}$. The universal form of low-energy eigenstates of H_{sp} for $g > \frac{\sqrt{2}}{2}$ is $|\phi_{sp}^{m,n}(g)\rangle = U_\theta^\dagger U_{\tilde{s}}^\dagger |m,n\rangle_{a,b}|\downarrow\rangle$. Note that $|\phi_{G,sp}\rangle = D_a^\dagger D_b^\dagger U_{\tilde{T}}^\dagger U_\theta^\dagger U_{\tilde{s}}^\dagger |0,0\rangle_{a,b}|\downarrow\rangle$ is the ground state in superradiant phase, where $U_{\tilde{T}} = e^{\frac{\tilde{s}}{\Omega}(a^\dagger + a + b^\dagger + b)(\sigma_+ - \sigma_-)}$, and the ground-state energy is $E_{0,sp} = \frac{\omega_0}{2}\sqrt{1-\frac{1}{4g^4}} - \frac{\omega_0}{2} - \frac{\Omega}{2}(g^2 + \frac{1}{4g^2})$.

Therefore the ground-state solutions of H demonstrate that quantum phase transition occurs at the critical point $g_c = \frac{\sqrt{2}}{2}$. This result is very different from the standard Rabi model whose critical point is $g_c = 1$ [19], meaning that the critical coupling strength needed in quantum phase transition becomes smaller as the number of field modes increases. The physics behind this is that the coupling between the qubit and each oscillator equally contributes to the critical point, and more field modes can provide more excitations for the ground state at the same coupling strength. The validity of the above diagonalized method is checked in Fig. 2. The result shows that relative error of ground-state energy quickly decreases to 10^{-3} even when $\Omega = 100\omega_0$. Note that contributions of a and b modes are symmetrical in both H_{np} and H_{sp}. The use of squeezed operator $e^{\frac{s}{2}(b^{\dagger 2} - b^2)}$ and $e^{\frac{\tilde{s}}{2}(b^{\dagger 2} - b^2)}$ for b mode instead of $e^{\frac{s}{2}(a^{\dagger 2} - a^2)}$ and $e^{\frac{\tilde{s}}{2}(a^{\dagger 2} - a^2)}$ for the a mode leads to the same quantum phase transition.

The rescaled photon number of the $a(b)$ mode $n_{c,a} = \frac{\omega_0}{\Omega}\langle\phi_{np}^{0,0}(g)|a^\dagger a|\phi_{np}^{0,0}(g)\rangle[n_{c,b} = \frac{\omega_0}{\Omega}\langle\phi_{np}^{0,0}(g)|b^\dagger b|\phi_{np}^{0,0}(g)\rangle]$ is 0 for $g < g_c$ and $n_{c,a} = \frac{\omega_0}{\Omega}\langle\phi_{sp}^{0,0}(g)|a^\dagger a|\phi_{sp}^{0,0}(g)\rangle[n_{c,b} = \frac{\omega_0}{\Omega}\langle\phi_{sp}^{0,0}(g)|b^\dagger b|\phi_{sp}^{0,0}(g)\rangle]$ is $\frac{1}{4g^2}(g^4 - g_c^4)$ for $g > g_c$; therefore $n_{c,a}$ and $n_{c,b}$ are two order parameters, as plotted in Fig. 3(a). Based on a variational method in the Appendix, the finite-frequency correction for $n_{c,a}(n_{c,b})$ is $n_{c,g_c} = \frac{1}{12}(\frac{2\Omega}{3\omega_0})^{-\frac{2}{3}}$, which is compared with the numerical solution in Fig. 3(b). The discrepancy between analytical and numerical solutions in Fig. 3(b) vanishes when $\frac{\Omega}{\omega_0} \gg 1$, demonstrating the validity of effective Hamiltonians H_{np} and H_{sp}.

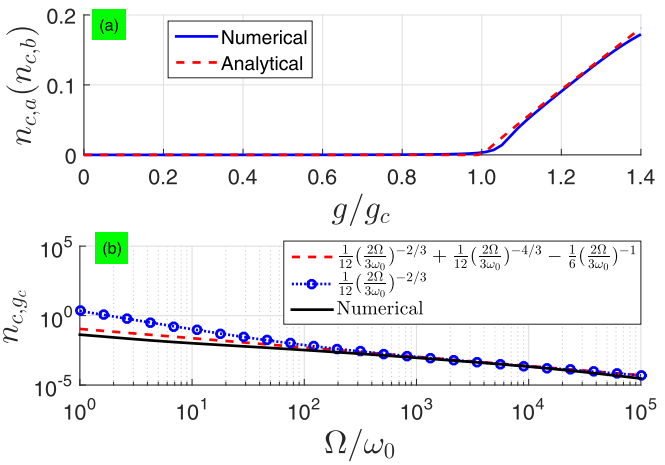

FIG. 3. (a) The rescaled photon number $n_{c,a}(n_{c,b})$ as a function of $\frac{g}{g_c}$ for the ground state with numerical (the blue-solid line) and analytical (the red-dotted line) results when $\Omega = 100\omega_0$. (b) The finite-frequency correction n_{c,g_c} as a function of $\frac{\Omega}{\omega_0}$ with analytical and numerical solutions at the critical point. The units of horizontal coordinate and vertical coordinate are dimensionless and ω_0, respectively.

The rescaled ground-state energy E_0 is $-\frac{\omega_0}{2}$ for $g \leqslant g_c$ and $-\frac{\omega_0}{2}[g^2 + (2g)^{-2}]$ for $g > g_c$, which is continuous at the critical point. However, its second-order derivative $\frac{d^2E_0}{dg^2}$ is zero for $g \leqslant g_c$ and $-\omega_0[1 + 12(2g)^{-4}]$ for $g > g_c$, which is discontinuous at the critical point, as plotted in Fig. 4(a). The finite-frequency correction for E_0 is $E_{0,g_c} = \frac{\omega_0}{4}(\frac{2\Omega}{3\omega_0})^{-\frac{4}{3}}$, which quickly decreases as $\frac{\Omega}{\omega_0}$ increases as shown in Fig. 4(b). This result reveals the second-order characteristics of the quantum phase transition in the ground state.

When g approaches g_c, excitation energies $\epsilon_{np,a}$ and $\epsilon_{sp,a}$ both vanish as a parabolic relation $|g - g_c|^{\frac{1}{2}}$ in the a oscillator, but the excitation energies $\epsilon_{np,b}$ and $\epsilon_{sp,b}$ do not vanish and both remain to be ω_0 in the b oscillator, as shown in Fig. 5.

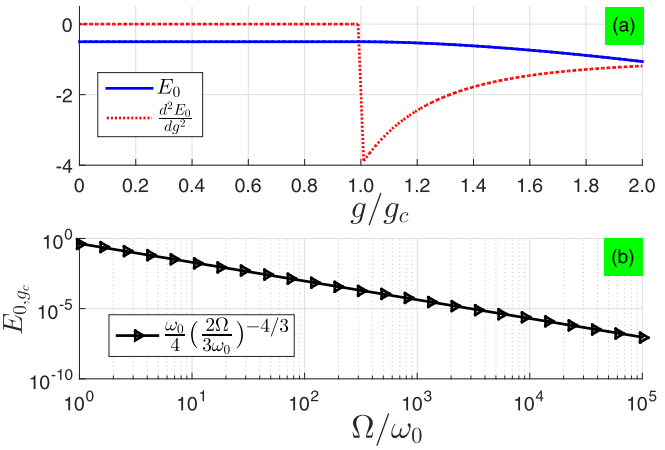

FIG. 4. (a) The analytical solution of ground-state energy E_0 (the blue-solid line) and its second-order derivative $\frac{d^2E_0}{dg^2}$ (the red-dotted line) as functions of $\frac{g}{g_c}$ when $\Omega = 100\omega_0$. (b) The finite-frequency correction E_{0,g_c} as a function of $\frac{\Omega}{\omega_0}$. The units of horizontal coordinate and vertical coordinate are dimensionless and ω_0, respectively.

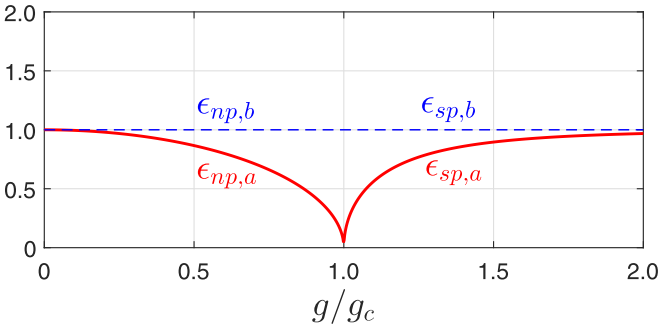

FIG. 5. Excitation energies ($\epsilon_{np,a}$, $\epsilon_{sp,a}$, $\epsilon_{np,b}$, and $\epsilon_{sp,b}$) as functions of $\frac{g}{g_c}$. $\epsilon_{np,a}$ and $\epsilon_{sp,a}$ are denoted by the red solid line. $\epsilon_{np,b}$ and $\epsilon_{sp,b}$ are denoted by the blue dashed line. The units of horizontal coordinate and vertical coordinate are dimensionless and ω_0, respectively.

III. QUENCH DYNAMICS

To investigate the quench dynamics of this system, we consider a time-dependent coupling parameter g, where g linearly increases with time t, i.e., $g(t) = g_f t/\tau$ (g_f is a final coupling strength and τ is the quench time). When the quench is slow enough and the system is initially in the ground state, the residual energy E_r at the end of the quench has an inverse-square relation with τ,

$$E_r = \tau^{-2}\frac{g_f^4}{4\omega_0(1-2g_f^2)^{\frac{5}{2}}} \propto \tau^{-2}. \tag{6}$$

When the quench ends at the critical point, i.e., $g_f = g_c$, the energy-gap equation becomes

$$g \simeq g_c - 2^{-\frac{13}{6}}(\omega_0\tau)^{-\frac{2}{3}}, \tag{7}$$

which leads to a universal scaling relation between E_r and τ:

$$E_r \simeq 2^{-\frac{8}{3}}\omega_0^{\frac{2}{3}}\tau^{-\frac{1}{3}} \propto \tau^{-\frac{1}{3}}. \tag{8}$$

This universal scaling between residual energy and quench time from $\tau^{-\frac{1}{3}}$ to τ^{-2} is the same with the standard Rabi model [19].

For the finite-frequency case, the motion equations are written as $i\dot{a}(t) = [a(t), \tilde{H}_{np}(t)]$ and $i\dot{b}(t) = [b(t), \tilde{H}_{np}(t)]$ in the Heisenberg picture, which leads to the following four coupled differential equations:

$$\begin{aligned}
i\frac{du_a(t)}{dt} &= \omega_0[(1-g(t)^2)u_a(t) - g(t)^2 v_a(t)] \\
&\quad + \frac{3\omega_0^2 g(t)^4}{\Omega}(u_a(t)+v_a(t))|u_a(t)+v_a(t)|^2, \\
-i\frac{dv_a(t)}{dt} &= \omega_0[(1-g(t)^2)v_a(t) - g(t)^2 u_a(t)] \\
&\quad + \frac{3\omega_0^2 g(t)^4}{\Omega}(u_a(t)+v_a(t))|u_a(t)+v_a(t)|^2, \\
i\frac{du_b(t)}{dt} &= \omega_0 u_b(t), \\
-i\frac{dv_b(t)}{dt} &= \omega_0 v_b(t),
\end{aligned} \tag{9}$$

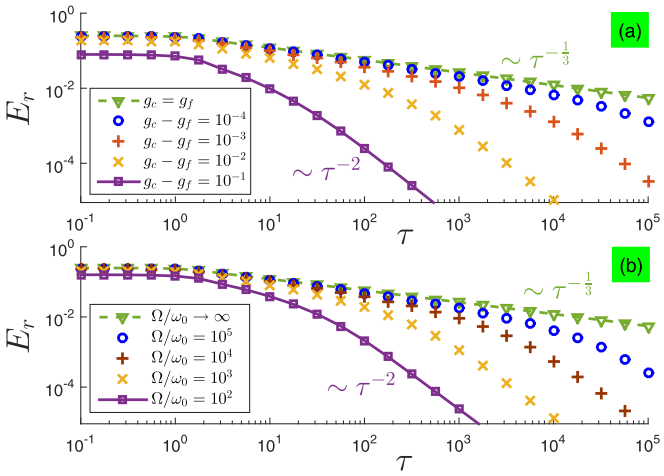

FIG. 6. Residual energy E_r as functions of the quench time τ obtained from Eq. (A41) for subfigure (a) when $\frac{\Omega}{\omega_0} \to \infty$ and Eq. (10) for subfigure (b) when $g_f = g_c$. The units of horizontal coordinate and vertical coordinate are $\frac{1}{\omega_0}$ and ω_0, respectively.

where $u_a(t)$, $v_a(t)$, $u_b(t)$, and $v_b(t)$ are four parameters to be determined. When the quench ends at time τ, the residual energy becomes

$$\begin{aligned}
E_r &= \omega_0(|v_a(\tau)|^2 + |v_b(\tau)|^2) - \frac{\omega_0 g_c^2}{2}|u_a(\tau)+v_a(\tau)|^2 \\
&\quad + \frac{3\omega_0^2 g_c^4}{4\Omega}|u_a(\tau)+v_a(\tau)|^4 + \frac{\omega_0^2 g_c^2}{4\Omega} + \frac{\omega_0}{2} \\
&\quad - \frac{\Omega}{4}\left(\frac{2\Omega}{3\omega_0}\right)^{-\frac{4}{3}} - \frac{\Omega}{18}\left(\frac{2\Omega}{3\omega_0}\right)^{-2}.
\end{aligned} \tag{10}$$

Detailed derivations from Eq. (6) to Eq. (10) can be seen in the Appendix. In Fig. 6, we plot residual energy E_r as functions of the quench time τ for different final coupling strengths g_f and different ratios $\frac{\Omega}{\omega_0}$. For small values of τ, the curves of E_r keep flat and suddenly increases as τ increases further. For large values of τ, when $\frac{\Omega}{\omega_0} \to \infty$ and $g_f = g_c$, the relation $E_r \sim \tau^{-\frac{1}{3}}$ is well satisfied, which is predicted by the universal scaling relation in Eq. (8). This result also confirms the universal adiabatic dynamics of quantum phase transition in the two-mode Rabi model. In Fig. 6(a), when g_f is gradually away from the critical point g_c, the universal scaling $\tau^{-\frac{1}{3}}$ progressively transforms to τ^{-2}, which is predicted by the universal scaling relation in Eq. (6). When the main finite-frequency correction $\frac{3\omega_0^2 g(t)^4}{\Omega}(u_a(t)+v_a(t))|u_a(t)+v_a(t)|^2$ is considered and the ratio $\frac{\Omega}{\omega_0}$ is gradually away from the infinity, this crossover behavior between residual energy and quench time is also observed in Fig. 6(b). This is because energy gap at the critical point opened by a finite ratio $\frac{\Omega}{\omega_0}$ has an equivalent effect with that opened by a deviation $|g_c - g_f|$ from the critical point.

IV. CONCLUSION

To summarize, when the ratio of the qubit transition frequency to the oscillator frequency approximates infinity, we have studied the second-order quantum phase transition and

the quench dynamics of the two-mode Rabi model based on the diagonalization approach. This approach jointly uses a beam-splitter operator and a squeezed operator for each effective two-mode Hamiltonian in the normal and superradiant phases. Analytical eigenstate and eigenenergy of the normal and superradiant phases are given. We find the special unitary transformation mapping the original Hamiltonian into two solvable two-mode Hamiltonians and demonstrate that there exists a critical point $g_c = \frac{\sqrt{2}}{2}$ where the second-order quantum phase transition happens. Compared with the standard Rabi model, this critical point means that the requirement of coupling strength between the qubit and two oscillators is largely loosened by joint effect of two modes. Based on the numerical simulation and analytical solution, we prove that the universal scaling between residual energy and quench time from $\tau^{-\frac{1}{3}}$ to τ^{-2} in the two-mode Rabi model is the same with that in the standard Rabi model. This diagonalization approach can also be generalized to any Rabi model, including two oscillators, for example, the dissipative two-mode Rabi model, which will largely motivate research in the new direction of quantum phase transitions for the multimode Rabi model.

ACKNOWLEDGMENTS

This work is supported by the National Natural Science Foundation of China (Grants No. 11705030, No. 11874114, No. 12074070, and No. 11875108) and the Natural Science Foundation of Fujian Province (Grants No. 2021J01574 and No. 2020J01471).

APPENDIX : DETAILS OF DIAGONALIZATION METHOD

In this section details of the diagonalization method are derived. The two-mode Rabi Hamiltonian of Eq. (1) can be written as

$$H = H_0 - \lambda V, \tag{A1}$$

where

$$H_0 = \omega_0(a^\dagger a + b^\dagger b) + \frac{\Omega}{2}\sigma_z, \tag{A2}$$

and

$$V = (a^\dagger + a + b^\dagger + b)\sigma_x. \tag{A3}$$

H_0 is an unperturbed Hamiltonian, which has two decoupled qubit subspaces $\{|\downarrow\rangle\}$ and $\{|\uparrow\rangle\}$. For $\frac{\Omega}{\omega_0} \gg 1$, the low-energy eigenstates of H_0 are restricted in $\{|\downarrow\rangle\}$, where there are only two simple harmonic oscillators. To find a unitary transformation $U_T = e^T$ to decouple the virtual transition between $\{|\downarrow\rangle\}$ and $\{|\uparrow\rangle\}$ induced by the interaction Hamiltonian V, we use the Schrieffer-Wolff transformation [19],

$$H_T = U^{-T} H U^T = \sum_{k=0}^{\infty} \frac{[H, T]^{(k)}}{k!}, \tag{A4}$$

where the special anti-Hermitian operator T is found to have an approximate form

$$T \simeq \frac{\lambda}{\Omega}(a^\dagger + a + b^\dagger + b)(\sigma_+ - \sigma_-) - \frac{4\lambda^3}{3\Omega^3}(a^\dagger + a + b^\dagger + b)^3(\sigma_+ - \sigma_-). \tag{A5}$$

With this choice for T, the transformed Hamiltonian approximately develops into

$$\widetilde{H}_T \simeq \omega_0(a^\dagger a + b^\dagger b) + \frac{\Omega}{2}\sigma_z + \frac{\lambda^2}{\Omega}(a^\dagger + a + b^\dagger + b)^2\sigma_z - \frac{\lambda^4}{\Omega^3}(a^\dagger + a + b^\dagger + b)^4\sigma_z + \frac{\omega_0\lambda^2}{\Omega^2}. \tag{A6}$$

For the $\frac{\lambda}{\Omega} \to 0$ limit and $\widetilde{H}_T$ is projected to $\{|\downarrow\rangle\}$, an effective Hamiltonian for two coupled oscillators in the normal phase is obtained,

$$H_{np} \simeq \omega_0(a^\dagger a + b^\dagger b) - \frac{\lambda^2}{\Omega}(a^\dagger + a + b^\dagger + b)^2 - \frac{\Omega}{2}, \tag{A7}$$

which is Eq. (4) of the main text.

To diagonalize H_{np}, we use a beam-splitter operator $U_\theta = e^{\theta(a^\dagger b - a b^\dagger)}$ and a squeezed operator $U_s = e^{\frac{s}{2}(a^{\dagger 2} - a^2)}$, where θ and s are two undetermined parameters. When U_θ acts on H_{np}, the transformed Hamiltonian becomes

$$\begin{aligned} H_\theta &= U_\theta H_{np} U_\theta^\dagger \\ &= \omega_0(a^\dagger a + b^\dagger b) - \frac{\lambda^2}{\Omega}[(\cos\theta + \sin\theta)(a^\dagger + a) \\ &\quad + (\cos\theta - \sin\theta)(b^\dagger + b)]^2 - \frac{\Omega}{2}. \end{aligned} \tag{A8}$$

When the condition $\cos\theta = \sin\theta$ is satisfied, i.e., $\theta = \frac{\pi}{4}$, only the a oscillator's Hamiltonian has a two-photon interaction, but the b oscillator's Hamiltonian already has been diagonalized. To further diagonalize the a oscillator's Hamiltonian, U_s is applied to H_θ leading to

$$\begin{aligned} H'_{np} &= U_s H_\theta U_s^\dagger \\ &= [\omega_0(\cosh^2 s - \sinh^2 s) - \frac{4\lambda^2}{\Omega}(\cosh s - \sinh s)^2] \\ &\quad \times a^\dagger a - [\omega_0 \cosh s \sinh s + \frac{2\lambda^2}{\Omega}(\cosh s - \sinh s)^2] \\ &\quad \times (a^{\dagger 2} + a^2) + \omega_0 b^\dagger b - \frac{\Omega}{2} - \omega_0 \sinh^2 s \\ &\quad - \frac{2\lambda^2}{\Omega}(\cosh s - \sinh s)^2. \end{aligned} \tag{A9}$$

With the choice of the squeezed parameter $s = \frac{1}{4}\ln(1 - 2g^2)$, the two-photon interaction vanishes and H_{np} is diagonalized as

$$H'_{np} = \omega_0\sqrt{1 - 2g^2}a^\dagger a + \omega_0 b^\dagger b + \frac{\omega_0}{2}\sqrt{1 - 2g^2} - \frac{\omega_0}{2} - \frac{\Omega}{2}, \tag{A10}$$

which is Eq. (5) of the main text.

If we use another beam-splitter operator $U_{\theta'} = e^{\theta'(a^\dagger b - a b^\dagger)}$ and a squeezed operator $U'_s = e^{\frac{s}{2}(b^{\dagger 2} - b^2)}$, where θ' is an undetermined parameter. When $U_{\theta'}$ acts on H_{np}, the transformed Hamiltonian becomes

$$\begin{aligned} H_{\theta'} &= U_{\theta'} H_{np} U_{\theta'}^\dagger \\ &= \omega_0(a^\dagger a + b^\dagger b) - \frac{\lambda^2}{\Omega}[(\cos\theta' + \sin\theta')(a^\dagger + a) \end{aligned}$$

$$+(\cos\theta' - \sin\theta')(b^\dagger + b)]^2 - \frac{\Omega}{2}. \tag{A11}$$

When the condition $\cos\theta' = -\sin\theta'$ is satisfied, i.e., $\theta' = -\frac{\pi}{4}$, only the b oscillator's Hamiltonian has a two-photon interaction, but the a oscillator's Hamiltonian already has been diagonalized. To further diagonalize the b oscillator's Hamiltonian, U_s' is applied to $H_{\theta'}$, leading to

$$\begin{aligned} H_{np}'' &= U_s' H_{\theta'} U_s'^\dagger \\ &= [\omega_0(\cosh^2 s - \sinh^2 s) - \frac{4\lambda^2}{\Omega}(\cosh s - \sinh s)^2] \\ &\quad \times b^\dagger b - [\omega_0 \cosh s \sinh s + \frac{2\lambda^2}{\Omega}(\cosh s - \sinh s)^2] \\ &\quad \times (b^{\dagger 2} + b^2) + \omega_0 a^\dagger a - \frac{\Omega}{2} - \omega_0 \sinh^2 s \\ &\quad - \frac{2\lambda^2}{\Omega}(\cosh s - \sinh s)^2. \end{aligned} \tag{A12}$$

With $s = \frac{1}{4}\ln(1-2g^2)$, the two-photon interaction vanishes and H_{np} is diagonalized as

$$H_{np}'' = \omega_0 a^\dagger a + \omega_0\sqrt{1-2g^2}\, b^\dagger b + \frac{\omega_0}{2}\sqrt{1-2g^2} - \frac{\omega_0}{2} - \frac{\Omega}{2}. \tag{A13}$$

To derive finite-frequency corrections for the Hamiltonian

$$\begin{aligned} \tilde{H}_{np} &= \langle\downarrow|\tilde{H}_T|\downarrow\rangle \\ &= \omega_0(a^\dagger a + b^\dagger b) - \frac{\lambda^2}{\Omega}(a^\dagger + a + b^\dagger + b)^2 \\ &\quad + \frac{\lambda^4}{\Omega^3}(a^\dagger + a + b^\dagger + b)^4 + \frac{\omega_0\lambda^2}{\Omega^2} - \frac{\Omega}{2}, \end{aligned} \tag{A14}$$

we propose a variational ground state $|\phi_{G,v}\rangle = e^{\frac{\pi}{4}(a^\dagger b - a b^\dagger)} e^{\frac{v}{2}(a^{\dagger 2} - a^2)}|0,0\rangle_{a,b}$ with a trial parameter v, which leads to the ground-state energy

$$\begin{aligned} E_{G,v} &= \langle\phi_{G,v}|\tilde{H}_{np}|\phi_{G,v}\rangle \\ &= \frac{\omega_0}{2}\cosh(2v) - \frac{2\lambda^2}{\Omega}e^{2v} + \frac{12\lambda^4}{\Omega^3}e^{4v} - \frac{\Omega}{2} + \frac{\omega_0\lambda^2}{\Omega^2}. \end{aligned} \tag{A15}$$

To find the minimum value of $E_{G,v}$, the following equation is calculated:

$$\frac{\partial E_{G,v}}{\partial v} = \frac{96\lambda^4}{\omega_0\Omega^3}e^{6v} + \left(1 - \frac{8\lambda^2}{\omega_0\Omega}\right)e^{4v} - 1 = 0, \tag{A16}$$

whose solution is $v_{\min} = \frac{1}{6}\ln(\frac{2\Omega}{3\omega_0})$ at g_c. Therefore the finite-frequency correction for $n_{c,a}$ is

$$\begin{aligned} n_{c,g_c} &= \frac{\omega_0}{\Omega}\langle\phi_{G,v}(v_{\min})|a^\dagger a|\phi_{G,v}(v_{\min})\rangle \\ &= \frac{1}{12}\left(\frac{2\Omega}{3\omega_0}\right)^{-\frac{2}{3}} + \frac{1}{12}\left(\frac{2\Omega}{3\omega_0}\right)^{-\frac{4}{3}} - \frac{1}{6}\left(\frac{2\Omega}{3\omega_0}\right)^{-1} \\ &\simeq \frac{1}{12}\left(\frac{2\Omega}{3\omega_0}\right)^{-\frac{2}{3}}, \end{aligned} \tag{A17}$$

which is the same with that for $n_{c,b}$. The finite-frequency correction for the rescaled ground-state energy is

$$\begin{aligned} E_{0,g_c} &= \frac{\omega_0}{\Omega}[\langle\phi_{G,v}(v_{\min})|\tilde{H}_{np}|\phi_{G,v}(v_{\min})\rangle - E_{0,np}] \\ &= \frac{\omega_0}{4}\left(\frac{2\Omega}{3\omega_0}\right)^{-\frac{4}{3}} + \frac{\omega_0}{18}\left(\frac{2\Omega}{3\omega_0}\right)^{-2} \\ &\simeq \frac{\omega_0}{4}\left(\frac{2\Omega}{3\omega_0}\right)^{-\frac{4}{3}}. \end{aligned} \tag{A18}$$

To derive the universal scaling of quench dynamics, similar to the procedure used in Ref. [19], we consider the normal-phase situation $g_f \leqslant g_c$ for simplicity, where g_f is a final coupling strength which satisfies the linearly time-dependent equality $g(t) = g_f t/\tau = \dot{g}t$. The time-dependent eigenstate of $H_{np}(g(t))$ is denoted as $|s_{np}(g(t)), n_a, n_b\rangle = e^{\frac{\pi}{4}(a^\dagger b - b^\dagger a)} e^{\frac{s_{np}(g(t))}{2}(a^{\dagger 2} - a^2)}|n_a, n_b\rangle$, whose eigenenergy is $\epsilon_{n_a,n_b}(g(t)) = \omega_0 n_a\sqrt{1-2g(t)^2} + \omega_0 n_b$. Therefore, the time-dependent wave function can be expanded as $|\Psi(t)\rangle = \sum_{n_a,n_b}\alpha_{n_a,n_b}(t)e^{-i\Theta_{n_a,n_b}(t)}|s_{np}(g(t)), n_a, n_b\rangle$, where $\Theta_{n_a,n_b}(t) = \int_0^t \epsilon_{n_a,n_b}(t')dt'$ and $\alpha_{n_a,n_b}(t)$ satisfies the Schrödinger equation,

$$\begin{aligned} \dot{\alpha}_{n_a,n_b}(t) = -\sum_{m_a,m_b}\alpha_{m_a,m_b}(t)\langle s_{np}(g(t)), n_a, n_b|\partial_t|s_{np}(g(t)), \\ m_a, m_b\rangle e^{i[\Theta_{n_a,n_b}(t) - \Theta_{m_a,m_b}(t)]}. \end{aligned} \tag{A19}$$

The solution of Eq. (A19) is

$$\begin{aligned} \alpha_{n_a,n_b}(g(t)) = -\sum_{m_a,m_b}\int_0^{g(t)} dg'\alpha_{m_a,m_b}(g')\langle s_{np}(g'), n_a, n_b|\partial_{g'} \\ |s_{np}(g'), m_a, m_b\rangle e^{i[\Theta_{n_a,n_b}(g') - \Theta_{m_a,m_b}(g')]}. \end{aligned} \tag{A20}$$

When the quench is slow, i.e., $\dot{g} << 1$, and the initial state of the system is ground state, i.e., $\alpha_{0,0}(0) = 1$ and $\alpha_{n_a,n_b}(0) = 0$ ($n_a, n_b \geqslant 1$), Eq. (A20) becomes

$$\begin{aligned} \alpha_{n_a,n_b}(g(t)) = -\int_0^g dg'\langle s_{np}(g'), n_a, n_b|\partial_{g'}|s_{np}(g'), 0, 0\rangle \\ \times e^{i[\Theta_{n_a,n_b}(g') - \Theta_{0,0}(g')]}. \end{aligned} \tag{A21}$$

Since the phase factor $e^{\frac{i}{\dot{g}}\int_0^{g(t)}[\epsilon_{n_a,n_b}(g') - \epsilon_{0,0}(g')]dg'}$ quickly oscillates, Eq. (A21) can be approximated as

$$\begin{aligned} \alpha_{n_a,n_b}(g(t)) \simeq i\dot{g}\frac{\langle s_{np}(g(t)), n_a, n_b|\partial_g|s_{np}(g(t)), 0, 0\rangle}{\epsilon_{n_a,n_b}(g(t)) - \epsilon_{0,0}(g(t))} \\ \times e^{i[\Theta_{n_a,n_b}(g(t)) - \Theta_{0,0}(g(t))]}\Big|_0^{g(t)}. \end{aligned} \tag{A22}$$

For $s_{np}(g(t)) = -\frac{1}{4}\ln(1-2g(t)^2)$, we find

$$\begin{aligned} &\langle s_{np}(g(t)), n_a, n_b|\partial_g|s_{np}(g(t)), 0, 0\rangle \\ &= -\frac{1}{2}\frac{\partial s_{np}}{\partial g}\langle n_a, n_b|(a^{\dagger 2} - a^2)|0,0\rangle \\ &= -\frac{\sqrt{2}g(t)\delta_{n_a,2}\delta_{n_b,0}}{2(1-2g(t)^2)}, \end{aligned} \tag{A23}$$

where the symbol δ represents the Delta function. Thus, only when $n_a = 2$ and $n_b = 0$ does α_{n_a,n_b} have a nonzero value, i.e.,

$$\alpha_{2,0}(g(t)) = \frac{-i\dot{g}g(t)}{2\sqrt{2}\omega_0(1-2g(t)^2)^{\frac{3}{2}}} e^{i[\Theta_{2,0}(g(t))-\Theta_{0,0}(g(t))]}, \tag{A24}$$

which leads to the residual energy at the end of the quench,

$$\begin{aligned} E_r(g_f) &= \sum_{n_a>0,n_b>0} \epsilon_{n_a,n_b}(g_f)|\alpha_{n_a,n_b}(g_f)|^2 \\ &\simeq \epsilon_{2,0}(g_f)|\alpha_{2,0}(g_f)|^2 \\ &= \tau^{-2}\frac{g_f^4}{4\omega_0(1-2g_f^2)^{\frac{5}{2}}} \\ &\propto \tau^{-2}. \end{aligned} \tag{A25}$$

According to the KZM mechanism [31], $g(t)$ should satisfy the energy-gap equation at the critical point,

$$\frac{1}{\eta(g(t))} = \left|\frac{\eta(g(t))}{\dot{\eta}(g(t))}\right|, \tag{A26}$$

where $\eta(g(t)) = 2\omega_0\sqrt{1-2g(t)^2}$, and $\dot{\eta}$ represents the η's first-order derivative as $g(t)$. Then we have the following equation:

$$(1-\sqrt{2}g(t))^{\frac{3}{2}} = \frac{g_f}{\omega_0\tau}g(t)(1+\sqrt{2}g(t))^{-\frac{3}{2}}. \tag{A27}$$

When the quench ends at the critical point, Eq. (A27) becomes

$$(1-\sqrt{2}g(t))^{\frac{3}{2}} \simeq \frac{2^{-\frac{5}{2}}}{\omega_0\tau}, \tag{A28}$$

i.e.,

$$g(t) \simeq g_c - 2^{-\frac{13}{6}}(\omega_0\tau)^{-\frac{2}{3}}. \tag{A29}$$

By replacing g_f in Eq. (A25) with $g(t)$ in Eq. (A29), the residual energy becomes

$$\begin{aligned} E_r &\simeq 2^{-\frac{8}{3}}\omega_0^{\frac{2}{3}}\tau^{-\frac{1}{3}} \\ &\propto \tau^{-\frac{1}{3}}. \end{aligned} \tag{A30}$$

To obtain the motion equation of quench dynamics, we first consider the $\frac{\Omega}{\omega_0} \to \infty$ limit. The effective time-dependent Hamiltonian in normal phase is

$$H_\theta(t) = \omega_0(a^\dagger a + b^\dagger b) - \frac{\omega_0 g(t)^2}{2}(a^\dagger + a)^2 - \frac{\Omega}{2}. \tag{A31}$$

In the Heisenberg picture, the motion equations can be written as $i\dot{a}(t) = [a(t), H_{np}(t)]$ and $i\dot{b}(t) = [b(t), H_{np}(t)]$. The time-dependent field mode operators can be expressed as

$$\begin{aligned} a(t) &= u_a(t)a + v_a^*(t)a^\dagger, \\ b(t) &= u_b(t)b + v_b^*(t)b^\dagger, \end{aligned} \tag{A32}$$

with an initial condition $u_a(0) = u_b(0) = 1$ and $v_a(0) = v_b(0) = 0$, which should satisfy the commutation conditions $|u_a(t)|^2 - |v_a(t)|^2 = 1$ and $|u_b(t)|^2 - |v_b(t)|^2 = 1$. The motion equations become

$$\begin{aligned} i\dot{u}_a(t)a + i\dot{v}_a^*(t)a^\dagger = \omega_0(v_a^*(t)a^\dagger + u_a(t)a) - \omega_0 g(t)^2[(u_a^*(t) \\ + v_a^*(t))a^\dagger + (u_a(t) + v_a(t))a] \end{aligned} \tag{A33}$$

and

$$i\dot{u}_b(t)b + i\dot{v}_b^*(t)b^\dagger = \omega_0(u_b(t)b + v_b^*(t)b^\dagger). \tag{A34}$$

By adding two commutation relations $[..., a^\dagger]$ and $[a, ...]$ ($[..., b^\dagger]$ and $[b, ...]$) to Eq. (A33) (Eq. (A34)), four coupled differential equations are obtained:

$$\begin{aligned} i\frac{du_a(t)}{dt} &= \omega_0[(1-g(t)^2)u_a(t) - g(t)^2 v_a(t)], \\ -i\frac{dv_a(t)}{dt} &= \omega_0[(1-g(t)^2)v_a(t) - g(t)^2 u_a(t)], \\ i\frac{du_b(t)}{dt} &= \omega_0 u_b(t), \\ -i\frac{dv_b(t)}{dt} &= \omega_0 v_b(t). \end{aligned} \tag{A35}$$

Then we consider the finite-frequency case. The effective time-dependent Hamiltonian with finite-frequency corrections in normal phase becomes

$$\begin{aligned} \tilde{H}_\theta(t) &= U_\theta \tilde{H}_{np}(t) U_\theta^\dagger \\ &= \omega_0(a^\dagger a + b^\dagger b) - \frac{\omega_0 g(t)^2}{2}(a^\dagger + a)^2 + \frac{\omega_0^2 g(t)^4}{4\Omega} \\ &\quad \times (a^\dagger + a)^4 + \frac{\omega_0^2 g(t)^2}{4\Omega} - \frac{\Omega}{2}. \end{aligned} \tag{A36}$$

By neglecting the nonlinear terms, the motion equations become

$$\begin{aligned} i\dot{u}_a(t)a + i\dot{v}_a^*(t)a^\dagger = \omega_0(v_a^*(t)a^\dagger + u_a(t)a) + [\frac{3\omega_0^2 g(t)^4}{\Omega} \\ \times |u_a(t) + v_a(t)|^2 - \omega_0 g(t)^2][(u_a(t) \\ + v_a(t))a + (u_a^*(t) + v_a^*(t))a^\dagger] \end{aligned} \tag{A37}$$

and

$$i\dot{u}_b(t)b + i\dot{v}_b^*(t)b^\dagger = \omega_0(u_b(t)b + v_b^*(t)b^\dagger), \tag{A38}$$

which lead to four coupled differential equations:

$$\begin{aligned} i\frac{du_a(t)}{dt} &= \omega_0[(1-g(t)^2)u_a(t) - g(t)^2 v_a(t)] \\ &\quad + \frac{3\omega_0^2 g(t)^4}{\Omega}(u_a(t) + v_a(t))|u_a(t) + v_a(t)|^2, \\ -i\frac{dv_a(t)}{dt} &= \omega_0[(1-g(t)^2)v_a(t) - g(t)^2 u_a(t)] \\ &\quad + \frac{3\omega_0^2 g(t)^4}{\Omega}(u_a(t) + v_a(t))|u_a(t) + v_a(t)|^2, \\ i\frac{du_b(t)}{dt} &= \omega_0 u_b(t), \\ -i\frac{dv_b(t)}{dt} &= \omega_0 v_b(t), \end{aligned} \tag{A39}$$

which is Eq. (9) of the main text. Compared with Eq. (A35), the main finite-frequency correction of Eq. (A39) is $\frac{3\omega_0^2 g(t)^4}{\Omega}(u_a(t) + v_a(t))|u_a(t) + v_a(t)|^2$.

In the $\frac{\Omega}{\omega_0} \to \infty$ limit, the time-dependent energy is

$$
\begin{aligned}
{}_{a,b}\langle 0,0|H_\theta(t)|0,0\rangle_{a,b} = \omega_0|v_a(t)|^2 - \frac{\omega_0 g(t)^2}{2}|u_a(t) \\
+v_a(t)|^2 - \frac{\Omega}{2}. \qquad \text{(A40)}
\end{aligned}
$$

When the quench ends at time τ, the residual energy becomes

$$
\begin{aligned}
E_r &= {}_{a,b}\langle 0,0|H_\theta(\tau)|0,0\rangle_{a,b} - E_{0,np}(\tau) \\
&= \omega_0(|v_a(\tau)|^2 + |v_b(\tau)|^2) - \frac{\omega_0 g_f^2}{2}|u_a(\tau) + v_a(\tau)|^2 \\
&\quad -\frac{\omega_0}{2}(\sqrt{1-2g_f^2} - 1). \qquad \text{(A41)}
\end{aligned}
$$

For the finite-frequency case, the energy at time t can be written as

$$
\begin{aligned}
{}_{a,b}\langle 0,0|\tilde{H}_\theta(t)|0,0\rangle_{a,b} &= \omega_0(|v_a(t)|^2 + |v_b(t)|^2) - \frac{\omega_0 g(t)^2}{2} \\
&\times |u_a(t) + v_a(t)|^2 - \frac{\Omega}{2} + \frac{3\omega_0^2 g^4(t)}{4\Omega} \\
&\times |u_a(t) + v_a(t)|^4 + \frac{\omega_0^2 g(t)^2}{4\Omega}. \qquad \text{(A42)}
\end{aligned}
$$

By using Eq. (A42) to subtract $\frac{\Omega}{\omega_0} \times$ Eq. (A18), the residual energy at the end of quench becomes

$$
\begin{aligned}
E_r &= \omega_0(|v_a(\tau)|^2 + |v_b(\tau)|^2) - \frac{\omega_0 g_c^2}{2}|u_a(\tau) + v_a(\tau)|^2 \\
&\quad + \frac{3\omega_0^2 g_c^4}{4\Omega}|u_a(\tau) + v_a(\tau)|^4 + \frac{\omega_0^2 g_c^2}{4\Omega} + \frac{\omega_0}{2} \\
&\quad - \frac{\Omega}{4}\left(\frac{2\Omega}{3\omega_0}\right)^{-\frac{4}{3}} - \frac{\Omega}{18}\left(\frac{2\Omega}{3\omega_0}\right)^{-2}, \qquad \text{(A43)}
\end{aligned}
$$

which is Eq. (10) of the main text.

[1] J. M. Fink, A. Dombi, A. Vukics, A. Wallraff, and P. Domokos, Observation of the Photon-Blockade Breakdown Phase Transition, Phys. Rev. X **7**, 011012 (2017).

[2] Z.-H. Sun, J.-Q. Cai, Q.-C. Tang, Y. Hu, and H. Fan, Out-of-time-order correlators and quantum phase transitions in the Rabi and Dicke models, Ann. Phys. **532**, 1900270 (2020).

[3] W. Casteels, R. Fazio, and C. Ciuti, Critical dynamical properties of a first-order dissipative phase transition, Phys. Rev. A **95**, 012128 (2017).

[4] H.-J. Zhu, K. Xu, G.-F. Zhang, and W.-M. Liu, Finite-Component Multicriticality at the Superradiant Quantum Phase Transition, Phys. Rev. Lett. **125**, 050402 (2020).

[5] L. Garbe, M. Bina, A. Keller, M. G. A. Paris, and S. Felicetti, Critical Quantum Metrology with a Finite-Component Quantum Phase Transition, Phys. Rev. Lett. **124**, 120504 (2020).

[6] R. Puebla, A. Smirne, S. F. Huelga, and M. B. Plenio, Universal Anti-Kibble-Zurek Scaling in Fully Connected Systems, Phys. Rev. Lett. **124**, 230602 (2020).

[7] X.-Y. Chen, Y.-Y. Zhang, L. Fu, and H. Zheng, Generalized coherent-squeezed-state expansion for the superradiant phase transition, Phys. Rev. A **101**, 033827 (2020).

[8] Y. Zhang, B.-B. Mao, D. Xu, Y.-Y. Zhang, W.-L. You, M. Liu, and H.-G. Luo, Quantum phase transitions and critical behaviors in the two-mode three-level quantum Rabi model, J. Phys. A: Math. Theor. **53**, 315302 (2020).

[9] P. Forn-Díaz, L. Lamata, E. Rico, J. Kono, and E. Solano, Ultrastrong coupling regimes of light-matter interaction, Rev. Mod. Phys. **91**, 025005 (2019).

[10] C. J. Zhu, L. L. Ping, Y. P. Yang, and G. S. Agarwal, Squeezed Light Induced Symmetry Breaking Superradiant Phase Transition, Phys. Rev. Lett. **124**, 073602 (2020).

[11] Y.-Z. Wang, S. He, L. Duan, and Q.-H. Chen, Quantum tricritical point emerging in the spin-boson model with two dissipative spins in staggered biases, Phys. Rev. B **103**, 205106 (2021).

[12] J. Leppäkangas, J. Braumüller, M. Hauck, J.-M. Reiner, I. Schwenk, S. Zanker, L. Fritz, A. V. Ustinov, M. Weides, and M. Marthaler, Quantum simulation of the spin-boson model with a microwave circuit, Phys. Rev. A **97**, 052321 (2018).

[13] M. Abdi, Dynamical quantum phase transition in Bose-Einstein condensates, Phys. Rev. B **100**, 184310 (2019).

[14] L. Garbe, I. L. Egusquiza, E. Solano, C. Ciuti, T. Coudreau, P. Milman, and S. Felicetti, Superradiant phase transition in the ultrastrong-coupling regime of the two-photon Dicke model, Phys. Rev. A **95**, 053854 (2017).

[15] K. Baumann, C. Guerlin, F. Brennecke, and T. Esslinger, Dicke quantum phase transition with a superfluid gas in an optical cavity, Nature (London) **464**, 1301 (2010).

[16] V. M. Bastidas, C. Emary, B. Regler, and T. Brandes, Nonequilibrium Quantum Phase Transitions in the Dicke Model, Phys. Rev. Lett. **108**, 043003 (2012).

[17] Q. Bin, X.-Y. Lü, T.-S. Yin, Y. Li, and Y. Wu, Collective radiance effects in the ultrastrong-coupling regime, Phys. Rev. A **99**, 033809 (2019).

[18] E. Clive and B. Tobia, Quantum Chaos Triggered by Precursors of a Quantum Phase Transition: The Dicke Model, Phys. Rev. Lett. **90**, 044101 (2003).

[19] M.-J. Hwang, R. Puebla, and M. B. Plenio, Quantum Phase Transition and Universal Dynamics in the Rabi Model, Phys. Rev. Lett. **115**, 180404 (2015).

[20] Q. Xie, H. Zhong, M. T. Batchelor, and C. Lee, The quantum Rabi model: Solution and dynamics, J. Phys. A: Math. Theor. **50**, 113001 (2017).

[21] M. L. Cai, Z. D. Liu, W. D. Zhao, Y. K. Wu, Q. X. Mei, Y. Jiang, L. He, X. Zhang, Z. C. Zhou, and L. M. Duan, Observation of a quantum phase transition in the quantum Rabi model with a single trapped ion, Nat. Commun. **12**, 1126 (2021).

[22] N. Wang, Z.-R. Gong, J. Lu, and L. Zhou, Phases transitions in a cross-cavity quantum Rabi model possessing PT symmetric structure, Front. Phys. **7**, 127 (2019).

[23] C. H. Alderete and B. M. Rodríguez-Lara, Cross-cavity quantum Rabi model, J. Phys. A: Math. Theor. **49**, 414001 (2016).

[24] L. T. Shen, J. W. Yang, Z. C. Shi, Z. R. Zhong, and C. H. Xu, Ground state of a cross-cavity quantum Rabi model, J. Phys. A: Math. Theor. **54**, 105302 (2021).

[25] F. J. Gómez-Ruiz, J. J. Mayo, and A. del Campo, Full Counting Statistics of Topological Defects After Crossing a Phase Transition, Phys. Rev. Lett. **124**, 240602 (2020).

[26] R. Puebla, S. Deffner, and S. Campbell, Kibble-Zurek scaling in quantum speed limits for shortcuts to adiabaticity, Phys. Rev. Research **2**, 032020(R) (2020).

[27] S. Felicetti and A. Le Boité, Universal Spectral Features of Ultrastrongly Coupled Systems, Phys. Rev. Lett. **124**, 040404 (2020).

[28] P. Titum and M. F. Maghrebi, Nonequilibrium Criticality in Quench Dynamics of Long-Range Spin Models, Phys. Rev. Lett. **125**, 040602 (2020).

[29] G.-Q. Zhang, Z. Chen, and J. Q. You, Experimentally accessible quantum phase transition in a non-Hermitian Tavis-Cummings model engineered with two drive fields, Phys. Rev. A **102**, 032202 (2020).

[30] D. Dolgitzer, D. Zeng, and Y. Chen, Dynamical quantum phase transitions in the spin-boson model, Opt. Express **29**, 23988 (2021).

[31] B. Dóra, M. Heyl, and R. Moessner, The Kibble-Zurek mechanism at exceptional points, Nat. Commun. **10**, 2254 (2019).

[32] N. K. Langford, R. Sagastizabal, M. Kounalakis, C. Dickel, A. Bruno, F. Luthi, D. J. Thoen, A. Endo, and L. DiCarlo, Experimentally simulating the dynamics of quantum light and matter at deep-strong coupling, Nat. Commun. **8**, 1715 (2017).